Constant chemical potential-quantum mechanical-molecular dynamics simulations of the graphene-electrolyte double layer

Constant Chemical Potential-Quantum Mechanical-Molecular Dynamics simulations of the Graphene-electrolyte double layer

Nicodemo Di Pasquale *[1], Aaron R. Finney[2], Joshua Elliott[3,4], Paola Carbone[3], and Matteo Salvalaglio[2]

[1] *Department of Chemical Engineering, Brunel University London, Uxbridge, UB8 3PH, United Kingdom*
[2] *Department of Chemical Engineering, University College London, London, WC1E 7JE, United Kingdom*
[3] *Department of Chemical Engineering, University of Manchester, Manchester, M13 9PL, United Kingdom*
[4] *Diamond Light Source, Harwell Science and Innovation Park, Didcot, Oxfordshire OX11 8UQ, United Kingdom*

October 2021

Abstract

We present the coupling of two frameworks—the pseudo-open boundary simulation method known as constant potential Molecular Dynamics simulations (CμMD), combined with QMMD calculations—to describe the properties of graphene electrodes in contact with electrolytes.

The resulting CμQMMD model was then applied to three ionic solutions (LiCl, NaCl and KCl in water) at bulk solution concentrations ranging from 0.5 M up to 6 M in contact with a charged graphene electrode. The new approach we are describing here provides a simulation protocol to control the concentration of the electrolyte solutions while including the effects of a fully polarizable electrode surface. Thanks to this coupling, we are able to accurately model both the electrode and solution side of the double layer and provide a thorough analysis of the properties of electrolytes at charged interfaces, such as the screening ability of the electrolyte and the electrostatic potential profile. We also report the calculation of the integral electrochemical double layer capacitance in the whole range of concentrations analysed for each ionic species, while the QM simulations provide access to the differential and integral quantum

*Corresponding author: nicodemo.dipasquale@brunel.ac.uk

capacitance. We highlight how subtle features, such as the adsorption of potassium at the interface or the tendency of the ions to form clusters, emerge from our simulations, contribute to explaining the ability of graphene to store charge and suggest implications for desalination.

1 Introduction

Interest in graphene-based devices has grown in recent years thanks to the versatility and physical characteristics of this new material, particularly for applications in which it is in contact with an electrolyte solution. The use of nanoporous graphene as a membrane for water desalination [1, 2] is one important example. The presence of pores of equal size to the electrolytes allows the selective passage of water through the membrane. Combined with the atomic scale thickness of graphene, this can lead to the creation of desalination membranes with higher performances than common polymer-based ones [3]. Another promising technologically relevant application is the use of graphene electrodes in electrochemical double layer (super)capacitor (EDLC) devices[4, 5, 6]. In fact, graphene [7, 8, 9, 10], porous activated carbon [11] and carbon nanotube [12, 13] electrodes potentially have relatively high charge storage capacity and a favourable specific energy to power ratio, due to rapid charge-discharge cycling [8] controlled by changes of an applied potential, together with lifetimes that can reach millions of cycles [11].

Typically, charge storage at carbonaceous electrodes is a non-faradaic process, where mobile ionic species accumulate at the interface between the electrode and the liquid phase. An important class of systems of this kind, which has gained lots of attention recently, is represented by cheap and easy-to-prepare aqueous-based electrolytes in contact with a graphene electrode [6]. Carbon-based EDLCs with aqueous-based electrolytes do not generally suffer from electrochemical degradation, can be non-toxic, and provide an attractive alternative solution to the problem of energy storage compared with traditional battery devices. Combined with a longer lifetime and high power density,[14] these energy storage systems could be increasingly applied to power small electronic devices and for acceleration and braking in electrical vehicles [5].

Several experimental works were undertaken to understand the physicochemical properties of neutral and charged graphene interfaces in contact with electrolyte solutions and to elucidate the nature of their charge storage capacity [15, 16, 17]. However, the delicate balance between hydration-free energy and surface effects, which regulate the physisorption of ionic species at surfaces, resulted in conflicting experimental findings (see [18] for a more detailed account). For instance, there are reports both supporting the conclusion that the capacitance of graphene films is ion-independent [16], as well as contrasting observations suggesting that basal capacitance is instead ion-specific (with, for example, a greater propensity for Na^+ and K^+ adsorption over Li^+ adsorption at negatively charged electrodes in the case of group I cations)[17]. Atomic-scale defects in the graphitic surface, its topography, dimensionality and chemical

modifications are difficult to control and have non-negligible effects in experimental measurements. As an example, mechanical cutting produces structural defects known as "dangling bonds" which modifies the measured capacitance of the sample [15, 19]. In this respect, a model of the graphene interface and its interactions with an electrolyte solution can exclude all the spurious effects originating from uncontrolled defects and chemical modification of the surface. Molecular modelling and simulations can help to improve understanding of the mechanisms involved in such complex systems and guide the interpretation of experimental results.

Many key features of supercapacitive devices are underpinned by the properties of the electrochemical double layer and their responses to electrode charging. Gouy-Chapman theory [20, 21] describes the double layer as a diffuse charged layer in the solution that compensates for an applied surface charge on the electrode. Modifications to this model include the adsorption of counter-ions at the surface in the so-called Stern layer [22]. The development of a mean-field theory based on the Poisson-Boltzmann lattice-gas model [23] has shown that features absent in the Gouy-Chapman theory, such as steric effects, ion correlations, and preferential adsorption [24, 25, 26] need to be accounted for in order to correctly describe the interactions between the ions and the electrode. Mechanistic insight for these effects and how they control charge storage can be gained from atomistic simulations of the graphene/electrolyte interface; these also enable the evaluation of ensemble properties, such as the free energy of adsorption of the ions at the interface [27]. Furthermore, simulations can establish the effect of solution concentration on ion accumulation at the electrode, their interfacial structure, and their dynamical properties.

In order to compare simulations with a macroscopic system, this adsorption should ideally be modelled in the presence of a bulk electroneutral solution with fixed composition to ensure a constant driving force for the adsorption at a charged surface. The bulk electroneutral solution can be obtained using constant chemical potential MD simulations, CμMD [28], which mimics open-boundary conditions, as shown in Finney et al. [29]. With CμMD, the authors simulated NaCl(aq) with concentrations spanning $\sim 0.1 - 10$ M in contact with a graphite surface. Their results indicate that the interface charge screening behaviour is a function of bulk solution concentration, with a transition (at $\sim$ 1M) from diffuse charge screening, qualitatively consistent with the picture from simple mean field models to a complex multi-layered structuring that systematically either over or under screens the surface potential. The multiple charged layers result from ion finite-size effects, over-compensation of the surface charge by oppositely charged ions closest to the surface, and non-idealities in solution, i.e., when the hypothesis of non-interaction between oppositely charged ions breaks down for large ions concentrations [30]. This last effect also has consequences on the conductance of the ions, which deviates from the prediction of the Nerst-Einstein equations [31].

Together with a constant driving force for ion adsorption from the bulk, another important effect to consider in the description of such systems is the polarisation of the electrode exerted by the adsorbing electrolytes [18]. Clas-

sical simulations typically model the non-bonded interactions between atoms within the electrolyte and atoms belonging to the interface using additive pairwise potentials such as the Lennard-Jones potential and Coulomb interactions between fixed point atom charges. Polarisation can be introduced using, e.g., oscillating charge models or by fitting short-range potentials to binding energies obtained from *ab initio* methods [27, 32, 33]. However, these models may not accurately capture the complex many-body effect associated with charge polarization at the electrode-solution interface. Another way to include polarisation in classical MD simulations is through the Constant Potential (CP) method first proposed in [34] and now popularized by the MetalWalls code [35]. The constant potential method has been successfully deployed to describe the properties of the electrochemical double layer of aqueous electrolytes and ionic liquids in contact with metal electrodes such as Au and Cu, nanoporous carbon electrode [36, 37], and non-planar electrode [14]. However, without further adaptations, the CP model relies on the approximation that the electrode is metallic and therefore able to perfectly screen charges, which is not the case for (semimetallic) graphene [18]. In recent advances, the Thomas-Fermi model was added to the CP model to tune the metallic character of the electrode allowing the description of imperfect conductors such as graphite [38]. Another advantage of the CP-related methodologies is the more straightforward connection with electrochemical experiments, which are usually run by fixing the potential difference of the electrodes [6].

Despite their successes, these models all rely on classical approximations. In order to describe quantities such as the density of states and electron density distribution in the presence of electrostatic potential arising from electrolyte configuration, we must include some electronic structure theory in the calculations. However, we want to highlight here that while any structure theory computation is, on average, more computationally expensive than a fully classical model, as we previously stated, it is needed to determine quantities otherwise non-accessible through a fully classical model. In this respect, we believe that since there is no one-size-fits-all model, the choice must be system- and resource-based, having clear in mind the strengths and limitations of each approach.

On the other hand, a full Quantum Mechanical (QM) treatment of the interactions between the electrolyte and the substrate is still unfeasible due to the length (tens of nm) and time (hundreds of ns) scales required for modelling the effect of the aqueous electrolytes. However, while the full QM model of the electrode/electrolyte system is out of reach, QM calculations can be used to compute a set of atomic partial charges on the electrode in the presence of the electrostatic potential arising from the position of the electrolyte atoms. This is exactly the spirit of our QMMD scheme, where QM calculations are coupled to MD simulations at fixed intervals of time integration. As such, the surface atom partial charges within the classical force field are updated on the fly. Such a QMMD scheme does not require any system dependent modifications to be applied for a specific system, as shown in [39], where the QMMD scheme was used without substantial variations for organic polymeric materials. In a more recent development, Machine Learning models have proven to be a viable option

in tuning the surface polarization if the scope of the system becomes too large for QM simulations. This is achieved by replacing the QM calculations with a Neural Network (NN) model trained to reproduce results from a wide range of QM calculations with varying distributions of electrolytes in solution. The NN acts as a polarizable-like force field, combining fast classical MD simulations with more accurate QM calculations of the interface polarization [40].

This present work leverages the QMMD framework introduced in [18] and the CμMD introduced in [28, 29]. The approach simultaneously captures surface polarization and concentration effects that can modify the structure and composition of the electrochemical double layer. We use the resulting CμQMMD protocol to examine interfaces between aqueous alkali chloride solutions at different concentrations with a graphene electrode surface, elucidating complex interfacial structure, dynamics, and electrochemical properties.

This paper is organized as follows: we first provide a brief overview of the QMMD and CμMD protocols, pointing to the relevant literature for the interested reader; we present the systems to which we apply the CμQMMD framework: a charged graphene electrode in contact with three different electrolyte solution, NaCl(aq), LiCl(aq), KCl(aq) at different concentrations. We derive the electrical properties of the interface in terms of the screening factor and electrical potential and calculate the total integral capacitance of this system by deriving the quantum and electrical double layer capacitance. Finally, we discuss the effects of complex solute speciation on the performance of graphene-electrolyte devices and draw some conclusions regarding this newly proposed simulation scheme.

2 Computational Models

In order to capture the dynamic polarization of a charged graphene surface in response to the evolving configuration of an electrolyte at a prescribed concentration, we coupled the classical CμMD simulation to the electronic structure theory calculations at regular time intervals. We provide a more detailed account of both models (CμMD and QMMD) in the following sections, while here, we will only discuss their coupling.

A sketch of the sequence of the operations involved is given in Figure 1. All the operations shown in Figure 1 are obtained through an in-house python wrapper. During the MD time integration obtained with GROMACS 2018.4 MD package [41], ion positions are passed to the Plumed software (v. 2.7) [42] patched with GROMACS, to compute the CμMD forces (see section 2.1 for more details). After the evolution of the atom positions, the final configuration of the electrolyte is extracted to compute the electrostatic potential. In turn, this latter quantity is used as input for the QM calculations obtained with the DFTB+ software package [43]. A more detailed description of the QM calculations are reported in our previous publications [44, 18]. From the QM results, the distribution of the charges on the graphene is extracted (see section 2.2 for more details) and used as input for the new iteration of the loop.

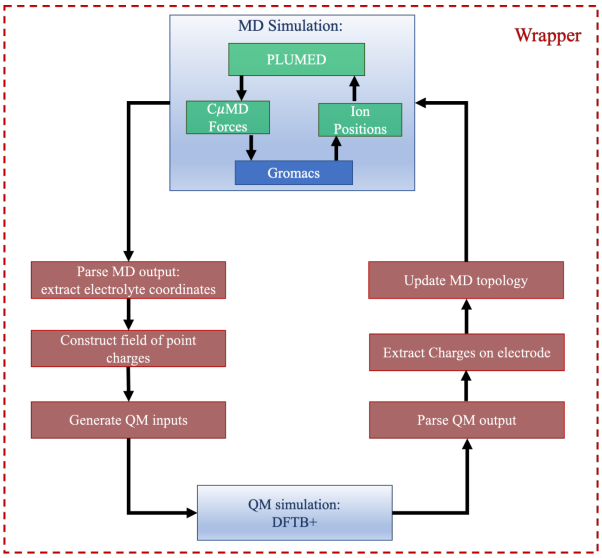

Figure 1: A representation of the computational workflow adopted in this work. In blue squares we placed the MD software and the QM software we considered, which, for the purpose of the python wrapper are called as external programs (i.e., we just take them as "black boxes"), whereas in red squares we are showing the operations included in the python wrapper.

2.1 CμMD Model

The graphene electrode we considered is located at $z = 0$ and is in contact with an electrolyte slab of thickness 8 nm. A further 8 nm of vacuum separates the system from its periodically repeating images. The electrolyte phase is divided into three regions: the first region starts at the graphene electrode up to a distance of 4 nm. The second one is the *control region*, which is used to control the concentrations. The third region is the *reservoir region* which provides the reservoir of ions to adjust the concentration of the electrolytes in the other regions. Figure 2 provides an example of the set-up adopted in this work, where we highlighted the different CμMD simulation cell regions.

The control of the concentration of the ions in solution is obtained by applying a force at the edge of the reservoir region according to a continuous function of the form,

$$F_i^{\mu}(z) = k_i(n_i^{\mathrm{CR}} - n_i^0)\left[\frac{1}{4\omega}\left(1 + \cosh\left(\frac{z - z_F}{\omega}\right)\right)^{-1}\right]. \qquad (1)$$

Here, ω was set to 0.2 nm and represents the width of the force region (between the control and reservoir regions highlighted by the blue lines in Figure 2) while k was 2×10^4 kJ mol^{-1} nm^{-1}, giving the correct densities in the bulk (see [29] for a discussion on these parameters). n^0 is the target ion number density,

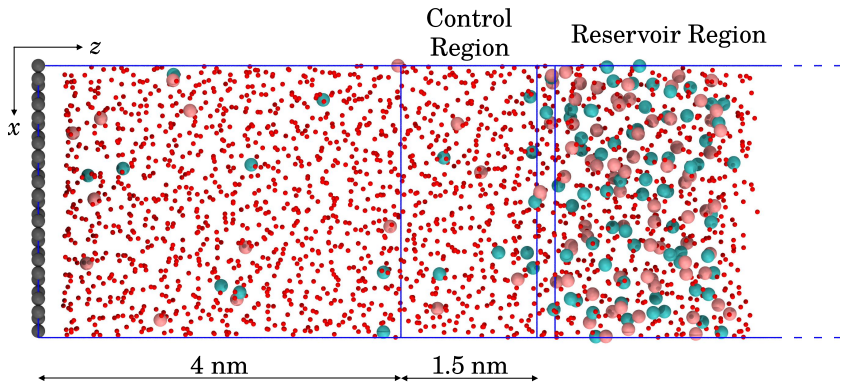

Figure 2: Example configuration from a CμQMMD simulation of KCl(aq) in contact with graphene in this work projected onto simulation x, z dimensions. K^+, Cl^-, O of water and C of graphene are shown by the pink, cyan, red and grey spheres. The blue lines highlight the CμQMMD control and reservoir regions, which also indicate the simulation cell boundaries. An extended vacuum region, around 8 nm in z, is truncated in the image.

while n^{CR} is the density calculated instantaneously during time integration in the control region. Finally, z_F is the position in z where the CμMD forces are applied. In our simulations, this is set to 5.5 nm beyond the graphene surface. Using this approach, the densities of cations and anions are constrained in the control region to maintain target concentrations of 0.5, 2.0, 3.0, 4.0, 4.4 and 6 M. At each MD time-step, ion positions are passed to Plumed in order to compute the CμMD forces only acting on those ions in the region of z_F. No external forces are applied to the ions outside this region, and any local change in the ion density at the interface results from the physical interactions between graphene and the solution.

2.2 QMMD Model

The generality of electronic structure theory and its ability to reproduce the electronic charge density distribution in semiconductors, metals, and semimetals implies that the QMMD approach can describe both long- and short-ranged redistribution of the surface charge induced by the presence of the electrolyte. Within each iteration of our scheme (see Figure 1), the fully classical system is taken as input for a quantum mechanical calculation. The simulation box is partitioned into surface atoms whose electronic structure is explicitly treated and electrolyte atoms that are converted into a set of point charges. The point charges take the values of the partial charges contained in the classical force field and form the background electrostatic potential during the computation of the electron structure (a sketch of this step is presented in Figure S.1 of the SI).

In order to describe the electronic structure of solid-electrolyte interfaces on the length scales required, we leverage the self-consistent charge Density Functional Tight-Binding (SCC-DFTB) [45] approach, which is an approximation to Kohn-Sham Density Functional Theory.

Upon derivation of the electronic structure, partitioning the charge density via Mulliken population analysis yields the surface atom partial charges, which are then passed to the classical force field. Finally, a short MD trajectory on the order of several picoseconds can be carried out (in the presence of the quantum mechanically polarized surface) to generate the electrolyte configuration for the following iteration. In our simulations, we employ a coupling between QM and MD calculations of 5 ps. We previously found for this class of systems that 5 ps represents a good compromise in terms of computational accuracy of the computed charges (0.004 e) vs computing time when compared with a QMMD simulation where the charges were updated at every MD time step [18].

2.3 Simulations Details

We will give in this section an account of the systems simulated, along with the numerical parameters considered in our work.

In our simulations, we consider a graphene electrode composed of 336 carbon atoms in contact with aqueous electrolyte solutions. We investigated three electrolyte systems, NaCl, KCl and LiCl, at concentrations ranging from 0.5 M to 6 M. However, due to the solubility limits of the KCl(aq) [46, 47], we limit the investigated concentrations to 4.4 M for the KCl system. These were target concentrations for the control region which we refer to throughout when discussing each system. An accurate evaluation of the bulk concentration requires sampling the mean ion density values in z far from the interface. At most, the deviation of the evaluated concentrations from the target ranges from 0.1 to 0.26 M across the concentration range we considered.

Our simulations are carried out at constant surface charge, which makes it difficult to draw comparisons across different electrodes since the potential applied is not necessarily constant. As such, when we compute the capacitance, we use the potential drop of the neutral electrode as a reference. This approach has been applied previously to compare the properties of the electrochemical double layer for different electrolytes [48]. Each operating condition was therefore repeated for two different total charges of the electrode: a charged graphene layer with a constant charge on the surface [49] σ of -0.449 e nm^{-2} (-0.0719 C/m^2) and a neutral one ($\sigma = 0$). In cases where $\sigma - 0.449$ e nm^{-2}, this corresponds to an overall charge on the electrode of -4 e; we accordingly added 4 cations to the system to compensate this surface charge.

It is important to highlight here that the whole loop represented in Figure 1 requires the interaction among three different software packages, Gromacs [41], PLUMED [42] and DFTB+ [43], and we will describe here the relevant parameters required in each case.

As described in section 2.2, in the QM part of the loop, we perform DFTB calculations which are obtained here using the DFTB+ software package [43].

The empirical description in our DFTB+ calculations of the interactions between the C atoms in the surface are described by the mio-1-1 parameter set [45]. The SCC charge threshold and Fermi temperature have been set to 1×10^{-2} Hartree and 300 K, respectively. Whereas, on first inspection, these criteria can be considered loose and should not be adopted for the calculation of the total electronic energy, rigorous testing in our previous works [18, 44] found that they provide a sufficiently accurate description of the surface charge distribution with respect to fully converged simulations, at a fraction of the computational cost. Finally, to compute the partial charges passed to the graphene force field at each MD step, we perform a Mulliken population analysis [50], which gives reasonable results for this class of systems[18, 44]. Mulliken charges ensure the full equivalence between the DFTB and classical forces acting on the electrolyte atoms as we verified in our previous work [18].

Molecular dynamics calculations in the NVT ensemble are carried out using GROMACS [51, 52], version 2018.4. The leapfrog algorithm with a timestep of 1 fs was used to integrate the equations of motion at a constant temperature of 298.15 K, controlled with the Nosé-Hoover thermostat, with a relaxation time of 1 ps. Long-range electrostatic interactions were treated using the particle-mesh Ewald approach, with a cut-off of 1.4 nm. Non-bonded interactions were computed using a Lennard-Jones 12-6 potential, truncated smoothly at 1.0 nm using a switch function starting at a distance of 0.99 nm. In all simulations, graphene carbon atoms were frozen, and water was modelled using the SPC/E model [53] with the SETTLE algorithm used to maintain rigid molecule geometries [54]. This choice is compatible with the Werder water-graphene parameters that reproduce the experimentally measured graphene/water contact angle [7, 55]. Ion force field parameters (for K^+, Li^+, Na^+, Cl^+), also compatible with the SPC/E model, are taken from the work of Joung and Cheatham [56]. At the beginning of the evolution, in systems at the higher end of the concentration range, many ions need to be stored into the reservoir. That, in turn, means that some water molecules and ions could easily escape in the vacuum if some bad contact is present. In order to prevent this effect, we added a fixed wall above the reservoir, interacting with water molecules and ions only through a short-range Lennard-Jones potential.

We equilibrated each system for 20 ns followed by 130 ns production runs to collect data for subsequent analyses of the steady-state structure of the interface. In all analyses discussed below, mean values and standard deviations (error bars) are obtained via averaging performed using 5 ns windows.

Structural analyses of the solutions are carried out using PLUMED [42] by post-processing the simulation trajectories. The first-shell coordination numbers is given by $N_{\mathrm{X-Y}}$, where $X = \{\mathrm{Na}^+, \mathrm{Li}^+, \mathrm{K}^+\}$ and $Y = \{\mathrm{Ow}, \mathrm{Cl}^-\}$. Therefore, $N_{\mathrm{X-Cl}}$ represents the first-shell coordination numbers for cations with anions, and $N_{\mathrm{X-Cl}}$ is the same quantity for cations with water oxygen atoms. N_{X-Y} is computed as $N_{X-Y} = \sum N^i_{\mathrm{X-Y}}$ where the index i indicates the i^{th} anion or water oxygen atom depending upon the type of coordination number being evaluated. In turn, $N^i_{\mathrm{X-Y}}$ is defined using a switching function for distances

larger than d_0:

$$N^i_{X-Y} = \begin{cases} e^{\left(\frac{-(r_i-d_0)^2}{2r_0^2}\right)}, & \text{if } r_i > d_0 \\ 1, & \text{otherwise} \end{cases} \quad (2)$$

r_i are distances between pairs of atoms; $r_0 = 0.01$ nm; and d_0 is the distance between a cation centre and the first minimum in radial distribution functions for the cations with anions or water oxygen atoms. We report the RDF for the different systems considered in Figure S.2 of the SI, from which we obtained $d_0 = 0.29$, 0.34 and 0.39 nm for Li– Na– and K–Cl. This ensured that a conservative definition of first-shell coordination was adopted in the analyses. Coordination numbers were evaluated in 1.3 nm regions in z closest to the graphene surface and 3.5 nm from the surface, representing the double layer and bulk solution regions, respectively. The first coordination sphere distributions for ions were used to construct a graph of ion-ion contacts using the NetworkX Python library [57]. This allowed us to identify and compute the size of the ion clusters formed. Ion clusters at the interface and within the bulk were identified by sampling the regions defined for computing the coordination numbers. Clusters were identified as fully connected networks in the graph of adjacent ion-ion connections according to this geometric criteria, regardless of their total charge or lifetime.

3 Results and Discussion

Thanks to the simulation protocol implemented, electroneutral solutions with fixed ion concentrations can be maintained in the Control Region in Figure 2, representing bulk solutions in equilibrium with the electrode-solution interfaces. This allows us to compare the behaviour of different electrolytes while controlling the electrolyte background concentration.

3.1 Density Profiles

We start this section by reporting in Figure 3 the (molar) concentration of the different ionic species in solution as a function of the z-coordinate, corresponding to the simulation cell direction orthogonal to the surface of negatively charged graphene electrodes. As expected, these profiles show preferential adsorption of cations at the electrode surfaces. For Na^+ and Li^+, a sharp density peak is observed at a distance of 0.5 nm from graphene, followed by a second, less pronounced peak at 0.75 nm. At the highest concentrations, a third cation peak emerges around 1.15 nm, which is more pronounced for Li^+. In contrast, in the case of K^+, a small peak at 0.3 nm is followed by a much larger and relatively diffuse density peak at 0.6 nm. This is due to specific adsorption of the larger cation at the carbon surface, a small number of which partially dehydrate to directly coordinate to carbon.

The difference in the z-density profiles for the different systems is less notable when considering Cl^- with respect to cations. At the lowest bulk concentrations,

there is a monotonically increasing density which reaches bulk values around 1.5 nm from the graphene interface. As the concentration rises, further density peaks are observed close to the carbon substrate, determined by the emergence of a multi-layered electrical double-layer structure, consistent with previously reported results [29, 18]. In such double-layer configurations, adjacent solution layers, rich in cations or anions, arise at the interface due to ion crowding (as in the case of the cations that are attracted towards the negatively charged surface of the electrode) and ion correlation (the localized positive excess charge in the closest layers to the electrode, in turn, attracts the anions).

The results reported in Figure 3 are consistent with those of [44] with NaCl(aq) and LiCl(aq) systems displaying, qualitatively, the same solution side double layer structure. The case of KCl(aq) differs somewhat. While the positions of the first two peaks (at 0.3 and 0.6 nm, see Figure 3c) that we obtained in our work is the same as the ones obtained in [44] for an analogous system, the intensity is sensibly different. In particular, our model predicts the majority of the K^+ are residing in the outer Helmholtz layer with a minority being absorbed on the interface, while results reported in [44] show that the majority of the K^+ are instead absorbed on the interface, and few of them resides in outer Helmholtz layer. This difference in the intensity of the peaks reflects the difference of the classical force-field used, in particular related to the fact that the force-field considered in [44] (i.e., the Madrid-2019 Force-Field [47]) considers scaled ionic charges and the K^+ ions have a smaller solvation free energy than the K^+ modelled with the force-field considered in this work [58]. The reduced strength of the interactions between the potassium and the water in the Madrid-2019 force-field makes the K^+ cation described in [44] more susceptible to dehydration and, therefore, more likely to be adsorbed on the interface.

Key differences between the adsorption behaviour of the ions is captured when polarisation of the electrode is accounted for. We have demonstrated this for two different force fields (here and [44]) which suggests that the behaviour is independent of the classical models. We note however, that while qualitatively similar, the different classical force-fields lead to different quantitative adsorption intensities of the K^+ ion on the surface - which can be linked to their slightly different classical free energies of hydration and ionic charge. On the other hand, other results in the literature (see [59]) show clear qualitative differences with our simulations (in particular for the KCl(aq) system where no adsorption is observed), most likely due to the lack of dynamic polarization considered for the graphene electrodes.

In turn, this brief account of the results in the literature shows the subtleties of discarding the polarizable nature of the electrode. Whenever polarization is considered, we observe the adsorption of K^+, implying that a non-polarizable model needs to be thoroughly checked, as it can change the physics of the model.

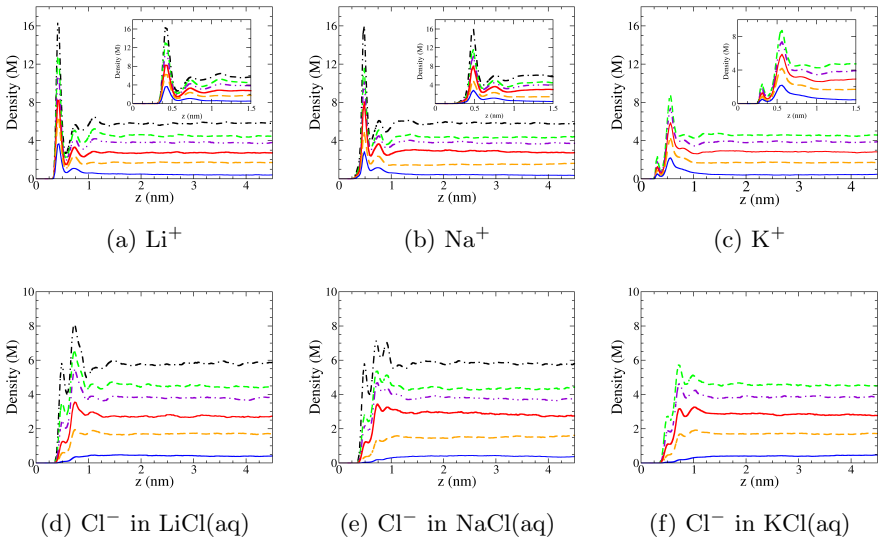

(a) Li^+ (b) Na^+ (c) K^+

(d) Cl^- in LiCl(aq) (e) Cl^- in NaCl(aq) (f) Cl^- in KCl(aq)

Figure 3: Molar (M) density of the cations (top row) and the corresponding anions (bottom row) for the three systems considered in this work. In the insets, the same results are shown for the region at 1.5 nm from the graphene electrode. The different curves are indicated as follows: Black dashed-dotted curve for a concentration of 6 M, green short-dashed curve for a concentration of 4.4 M, magenta double dotted-dashed curve for concentration of 4.0 M, solid red curve for a concentration of 3.0 M, orange long-dashed curve for a concentration of 2.0 M, and a solid blue curve for concentration of 0.5 M, respectively, where concentration refers to the bulk solution concentration. The colour code defined here will be valid for all the results shown in sections 3.1 and 3.2. We report the same pictures with error bars in Figures S.3-S.8 of the SI.

3.2 Electrical Double Layer Properties

In this section, we derive and analyze the electrical properties of the electrode-electrolyte systems considered in this work.

Electrode Charge Screeninig We begin by considering the screening factor [29] f defined as:

$$f(z) = -\int_0^z \frac{\rho_{ions}(z')}{\sigma} \mathrm{d}z' \tag{3}$$

where σ is the surface charge of the electrode interface and $\rho_{ions}(z)$ is the charge density of ions only, which is considered a function of just the z coordinate, i.e., it is averaged over the x and y coordinates.

The screening factor represents the extent to which the electrolyte phase electrically screens the charged interface. When f converges to a value of one, the charge on the electrode is entirely shielded by the electrolyte. Here, we include only the charges on ions when computing the solution charge density in z to facilitate a comparison with simple mean-field models, which often treat the solvent as a continuum field with defined permittivity. However, we report the screening factor calculated using the total density charge in Figures S.19-S.21 and Section S.2 of the SI.

The screening factors for all systems are reported in Figure 4. When the concentration of the ions is below 1 M, an under-screening near the interface can be observed. The screening factor f increases smoothly, reaching the value of one at around $z = 2$ nm. This is qualitatively consistent with the predictions of Gouy-Chapman's theory, where a diffuse double layer region with exponentially decreasing and increasing counter- and co-ion concentrations are predicted as a function of a monodimensional distance coordinate adjacent to a charged, planar surface. For higher concentrations, however, f transitions to over-screening at relatively small values of the z coordinate. The over-screening, highlighted by the first peak at $z \approx 0.6$ nm reported in Figures 4a to 4c, depends both on the particular ion and the bulk concentration. In particular, the LiCl system has the strongest over-screening effect on the electrode across the entire concentration range considered. When all solution charges are included in the determination of $\rho(z')$ in Equation (3), as shown in Figure S.20 of the SI, the over- and under-screening in the double layer is amplified, highlighting how the structuring of both ions and solvent and the finite size of molecules in solution layers should be included to properly account for the screening of the surface potential by the solution.

Over-screening is a well-known effect for ionic liquids [25] and is usually not considered important in the electrolyte solutions, as this was only apparent at relatively high concentrations [18, 29, 59]. The fact that over-screening appears for a higher concentration of the solute, in turn, can be linked directly to the structuring of the ions near the interface observed in Figure 3. With the increase in concentration, the density of the cations closest to the electrode increases with respect to their value in the solution bulk (see Figure 3). The

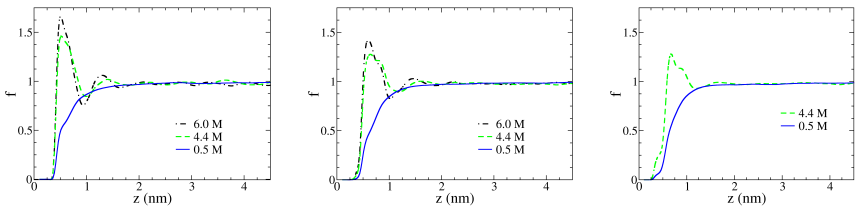

(a) LiCl (b) NaCl (c) KCl

Figure 4: Screening factor as defined in Equation (3) for the three systems considered using ions charge densities only. We included only a subset of the concentrations without error bars for clarity. The color scheme follows the convention defined in Figure 3. The results for all the concentrations along with error bars are reported in the SI (see Fig. S.9-S.11 of the SI).

excess charge associated with this ion accumulation is balanced in adjacent solution layers until the average bulk density is reached [14]. This description is consistent with our observations, where lithium and sodium show a high degree of structuring near the interface relative to potassium (i.e., multiple ion density peaks are observed, accompanied by a significant over-screening effect). In contrast, potassium, with the lowest degree of structuring near the interface, shows the smallest over-screening among the three ion solutions considered. Moreover, for potassium, we observe a variation in the slope of the screening factor when $z \approx 0.5$ nm, which increases (becoming more pronounced) as a function of concentration. This additional feature in the screening factor, absent in NaCl and LiCl, can be explained by the direct coordination of the K^+ (i.e., through the first coordination sphere) to carbon atoms (as also observed in [44]), as opposed to the behaviour of the cations in LiCl(aq) and NaCl(aq) systems (see the first peak at ≈0.35 nm in Figure 3c with respect to the first peak at ≈0.5 nm in Figures 3a and 3b).

Electrode Polarisation We will focus in this section on the K^+ ion, as it is the only one which is adsorbed on the graphene surface. The solvation free energy of the potassium is the lowest among the three cations [58]. Therefore, it is expected a greater ability of K^+ to lose (at least partially) its solvation cell with respect to Li^+ and Na^+. However, the smaller free energy by itself does not guarantee to observe such phenomena as we previously noted for the work of [60].

In a polarizable model of the interface, the approach of a positively charged cation to the (overall negative) interface greatly influences the distribution of the charges on the surface. In particular, when a cation is adsorbed on the surface, we can expect a stronger localization of negative charges near its position. We give an example of this behaviour in Figure 5 where we show the coordination of the K^+ with the carbon atoms on the graphene electrode for the lowest

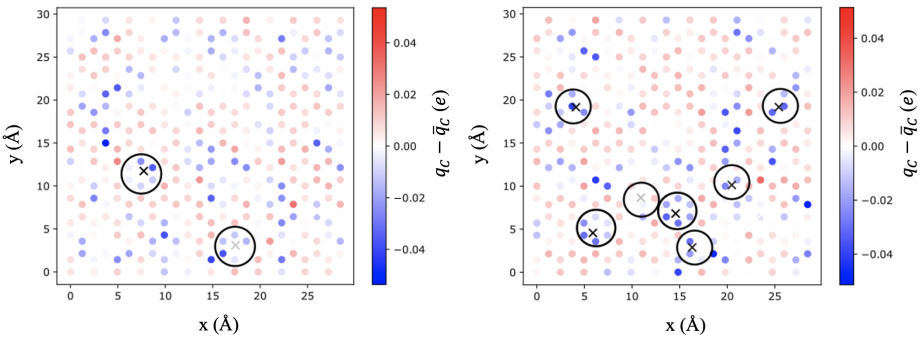

(a) 0.5 M (b) 4.4 M

Figure 5: Representative plot of the computed Mulliken charges on the graphene sheet charged with -4 e and in contact with kCl solutions at different concentrations. The results are given in terms of deviation from the average charge per carbon atom (given in this case by $\bar{q}_C = -4/336$ e, (where -4 e is the total charge of the graphene sheet composed by 336 carbon atoms). Circled X's mark the coordinates of K ions directly adsorbed on the surface.

(0.5 M) and the highest concentration (4.4 M) considered here. The plots in Figure 5 represent a single snapshot in the 150 ns long simulation with the highest number of potassium cations in direct contact with the interface (i.e., at a distance of 0.26 nm from the interface). As expected, the number of K^+ in direct contact with the interface increases as the bulk concentration of the cations increases, consistently with the observation in Figure 4 for the short-distance (from the electrode) behaviour of the screening factor, which increases with concentration. The accumulation of K^+ in the nearby region to the negative electrode (see Figure 3c) results in an increased non-uniformity of the partial charge distribution on the electrode, with higher negative charges located on the carbons closer to the coordinated K^+.

The feedback mechanisms just described, i.e., a cation with low solvation free energy approaches the interface in the electrical double layer, the localization of negative charges promotes the loss of water molecules, which allows the cation to move closer to the interface, which responds with a stronger localization of the negative charges is what makes the adsorption possible.

The results we have presented in this section show the importance of including the polarisation of the interface in a model to correctly capture the adsorption behaviour, however, more studies are needed to put these analyses on a more firm quantitative basis. We discussed a generic "low value" of the solvation free energy, which ensures adsorption when considered alongside a polarizable interface. It would be important to define such values quantitatively.

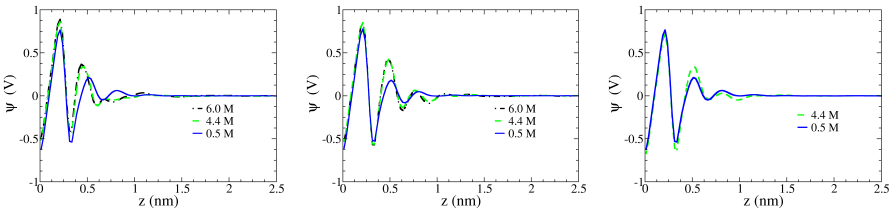

(a) LiCl (b) NaCl (c) KCl

Figure 6: Electrostatic potential as defined in Equation (5) for the three systems considered at the highest and lowest concentration for each system. We included only a subset of the concentrations for clarity. The color scheme follows the convention defined for Figure 3. The results for all the concentrations are reported in the SI (see Figures S.12-S.14 of the SI).

Electrical Potential in the Double Layer We calculated the electrical field $E(z)$ and the electrical potential, $\psi(z)$ in the direction orthogonal to the interface using the Poisson equation:

$$-\frac{\mathrm{d}^2\psi(z)}{\mathrm{d}z^2} = \frac{\mathrm{d}E(z)}{\mathrm{d}z} = \frac{\rho(z)}{\epsilon_0} \tag{4}$$

where $\rho(z)$ is the charge density calculated for all the atoms in the system calculated along the perpendicular axis to the electrode and ϵ_0 is the permittivity in vacuum. The electrical potential, ψ(z), is obtained from Equation (4) by integrating twice with respect to the z-coordinate:

$$\psi(z) = -\frac{1}{\epsilon_0}\int_0^z \int_0^{z'} \rho(\zeta)\mathrm{d}\zeta\mathrm{d}z' \tag{5}$$

The two integration constants in Equation (5) are chosen to set the electrostatic field and potential equal to zero in the bulk, which amounts to considering the bulk as the reference for the calculation of the electrostatic potential.

The results of Equation (5) are reported in Figure 6 for a selection of concentrations (see Figures S.12-S.14 of the SM for the entire range of concentrations). In stark contrast to the exponential behaviour predicted by models based on the Gouy-Chapman double layer theory, which treats the solvent medium as a continuum with known dielectric, atom/molecule finite-size effects give rise to an undulating $\psi(z)$ function in the interfacial region at all concentrations and in all systems. When calculating the charge distribution, we include all solution species, including the partial charges associated with the oxygen and hydrogen atoms in water molecules. Hence, it is unsurprising that the structuring of ions and water molecules at the interface gives rise to a significant departure from the predictions of simple mean field models. Indeed, these finite size effects are a well-reported feature of electrode-electrolyte systems [61, 62].

From a relatively large negative value of the potential at the electrode, the (partial) charges of ions and water give rise to fluctuations that attenuate at larger values of z, where the bulk solution behaviour is recovered. Generally, increasing the bulk solution concentration increases the amplitude of $\psi(z)$ fluctuations. Furthermore, it is evident from Figure 6a and Figure 6b that the crowding of ions in the double-layer increases with concentration as the positions of peaks and minima in z shift to lower values, a feature also observed by Finney et al. [29] with graphite and which was related to changes in the screening factor. This concentration dependence is less apparent in the case of KCl(aq), where the value of $\psi(z)$ at the first maximum is less susceptible to changes in the concentration as opposed to NaCl(aq) and LiCl(aq).

Electrical Double Layer Capacitance The total capacitance C_{TOT} in these kinds of systems is usually considered as composed of two independent components combined in series: the Electrochemical Double-Layer Capacitance (EDLC), C_{EDL}, and the quantum capacitance (or the space charge capacitance, C_Q), depending on the spatial distribution of the charges on the graphene [44]. The total capacitance is then given by

$$\frac{1}{C_{TOT}} = \frac{1}{C_{EDL}} + \frac{1}{C_Q} \tag{6}$$

From Figure 6 we can easily derive the potential drop, $\Delta\psi$, across the interface as* [44] $\Delta\psi = \Delta\psi^- - \Delta\psi_{ref}$ where $\Delta\psi^-$ and $\Delta\psi_{ref}$ represent the potential drop at the interface with respect to the bulk for the charged and neutral electrodes, respectively. As a reference for the calculation of the potential drop, we use the potential at the interface in a neutral electrode with all other conditions unchanged. We report the calculation of the potential across the system for a neutral electrode in the SI (see Figures S.15-S.17 of the SI) along with the potential drop at the interface both for the neutral electrode ($\Delta\psi_{ref}$) (see Table S.1 of the SI) and the charged electrode ($\Delta\psi^-$) (see Table S.2 of the SI). With this definition of the potential drop, the EDLC can be obtained, as

$$C_{EDL} = \frac{\sigma}{\Delta\psi} \tag{7}$$

The quantum capacitance instead is obtained by calculating the differential quantum capacitance C_Q^{diff} according to [44]:

$$C_Q^{diff}(\psi) = \frac{e^2}{4k_BT}\int_{-\infty}^{\infty}\left[D(E)\mathrm{sech}^2\left(E+\psi\right)\right]\mathrm{d}E \tag{8}$$

Where e is the electron charge, E is the energy relative to the Fermi level, $D(E)$ is the density of states at a given energy, k_B is the Boltzmann constant, and T is the temperature. By integrating the differential quantum capacitance

*A more precise notation for the potential drop across the interface would have been $\Delta\Delta\psi = \Delta\psi^- - \Delta\psi_{ref}$.

with respect to the potential ψ up to the potential drop $\Delta\psi$ calculated for each system, we obtain the integral quantum capacitance C_Q:

$$C_Q = \frac{1}{\Delta\psi}\int_0^{\Delta\psi} C_Q^{diff}(\psi)\mathrm{d}\psi \tag{9}$$

For more detailed information about the calculation of the quantum capacitance, we refer the reader to our previous work [44].

concentration	$\Delta\psi$	C_{EDL}	C_Q	C_{TOT}
	LiCl			
0.5	-0.995	7.20	10.15	4.21
2.0	-0.955	7.50	9.70	4.23
3.0	-0.952	7.52	9.66	4.23
4.0	-0.952	7.52	9.66	4.23
4.4	-0.941	7.61	9.54	4.23
6.0	-0.961	7.45	9.76	4.22
	NaCl			
0.5	-0.996	7.19	10.17	4.21
2.0	-0.964	7.43	9.81	4.23
3.0	-0.947	7.56	9.60	4.23
4.0	-0.945	7.58	9.58	4.23
4.4	-0.935	7.66	9.48	4.24
6.0	-0.954	7.51	9.68	4.23
	KCl			
0.5	-0.980	7.31	10.07	4.24
2.0	-0.958	7.48	9.73	4.23
3.0	-0.949	7.55	9.62	4.23
4.0	-0.934	7.67	9.46	4.24
4.4	-0.937	7.64	9.50	4.23

Table 1: Electrostatic potential drop ($\Delta\psi$) across the interface (in V), Electrochemical double layer capacitance C_{EDL}, Quantum Capacitance C_Q, and total capacitance C_{TOT} (in μF cm^{-2}) for each concentration considered (in M).

The results for C_Q, C_{EDL}, and C_{TOT} for all of the systems considered are reported in Table 1. The data show that the total capacitance is practically constant across the entire concentration range and for all solution types. The largest variation in C_{TOT} we obtained among all the systems is ≈2% (between the LiCl(aq) and KCl(aq) at 4.4 M). This result contrasts with the different behaviour of the three cations in solution and near the electrode interfaces, as highlighted in the discussion of the number density of ionic species at the

interface (see Figure 3) their screening effect on the charge of the electrode (Figure 4), and as further discussed in the following section in relation to their clustering properties.

An important point we want to highlight here is that such differences in the behaviour of the cation in solution can be correctly captured through the use of a simulation protocol that combines the pseudo-open boundary condition, i.e., CμMD, to maintain constant composition electroneutral bulk solutions beyond the double layer, and the quantum mechanical description for the distribution of partial charges of the electrode. However, while capacitance is a critical parameter for this kind of system's applications as supercapacitors, we showed here that the physics of the interfaces between graphene electrodes and electrolytes are much richer than the one captured by such a quantity.

3.3 Ion Association

An often overlooked effect in alkali chloride solutions is the tendency for ions to associate, forming clusters. Depending upon the operating conditions, these effects may have important implications when designing charge storage and desalination devices. Furthermore, a molecular-scale perspective of association as a function of concentration can inform electrode-solution models at larger scales that capture non-ideal solution effects. Even simple salt solutions exhibit significant non-ideal behaviour at high concentrations. Recent experiments [63] and simulations [64] have shown that extended liquid-like clusters exist in bulk NaCl(aq) at high concentrations, and the extent of these ionic networks is promoted in the double layer at carbon surfaces [29]. Since the effectiveness of the graphene-electrolyte devices often depends on the ability to 'build up the double layer' (i.e., accumulate ions from the bulk solution in the interfacial region), the structure and mobility of ion species can be essential to this.

Ion Clusters Figure 7 provides the average first-sphere coordination number between cations and O of water (see Figure 7a) as well as cations and anions for all systems, calculated using Equation (2). The results shown in Figure 7 indicate no significant surface effect on the coordination of cations with water or chloride when ions in the interface ($0 < z < 2.5$ nm) and bulk ($2.5 < z < 4.5$ nm) regions were investigated. There is a slight increase in the mean cation-anion coordination, and a concomitant decrease in cation-water coordination, at the interface compared to the bulk; however, this difference is within the margin of error. Generally, the effect of increasing concentration is to increase the number of cation-anion contacts, particularly for KCl(aq), where the coordination number is more than double that of the other systems for all concentrations (and with Li–Cl coordination being negligible even at 6 M). From the largest to smallest variation in the coordination number, we can write $K^+ \rightarrow Na^+ \rightarrow Li^+$. This trend follows the decrease of the ion radius and is likely due to the stronger water binding in the solvation spheres of smaller cations. Furthermore, the average cation-water coordination number is unchanging with a concentration within the margin of error.

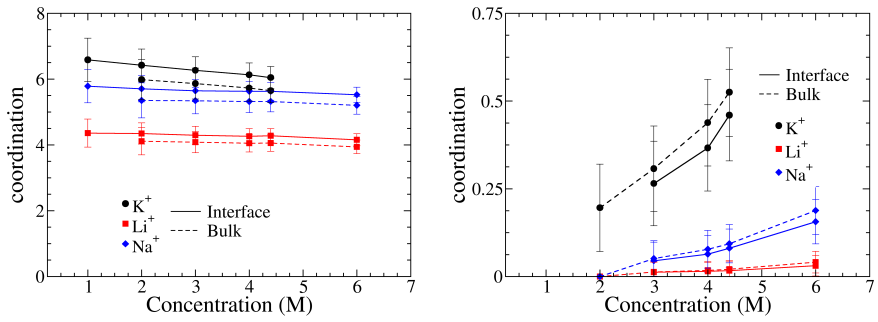

(a) Cation/Water (b) Cation/Anion

Figure 7: Coordination number for the different systems at the different concentrations.

In simulations of NaCl(aq) in contact with graphite, [29] the substrate was found to increase cation-anion correlations in the double layer with respect to the bulk, particularly beyond 5 M. It is important to note that different models (due to the different system) were used and also that system size likely plays a role in the extent that clusters can grow (both in, e.g., the system-size dependence of the availability of ions to form associates and the extent to which finite-size and percolating clusters may form in effectively confined canonical systems.)

The change in coordination for different salts is reflected in the cluster size probability distributions presented in Figure 8 for the case of 4.4 M (we report the results for the entire range of concentrations in Figure S.18 of the SM). There is a clear difference in the extent to which clusters can grow, with lithium forming clusters containing at most four ions and potassium forming much larger networks containing as many as 35 ions. Even at the highest concentrations, the majority of the Li^+ are dispersed in solution, fully solvated in their first shell. A snapshot of a configuration obtained during the simulation of KCl at 4.4 M is shown in Figure 8. Although the most probable clusters contain only a few ions (for clusters composed of five ion units, we obtained a relative frequency of 0.01), larger species contribute to the charge storage capacity and must be considered. What we observe is a stronger tendency of the potassium to associate into large aggregates—albeit ones which are highly dynamic on the timescales of the simulations—compared to sodium or lithium.

Since the KCl(aq) system shows the formation of large aggregates of ions, it is interesting to study the relative frequency of the charge of these aggregates. In Figure 9, we plot the 2-dimensional histogram showing the relative frequencies of the charge vs. the cluster size for the KCl(aq) system. The histogram is skewed towards positive charges, with the appearance of clusters containing an excess of positive charge as large as +7e, although the majority of the clusters are neutral.

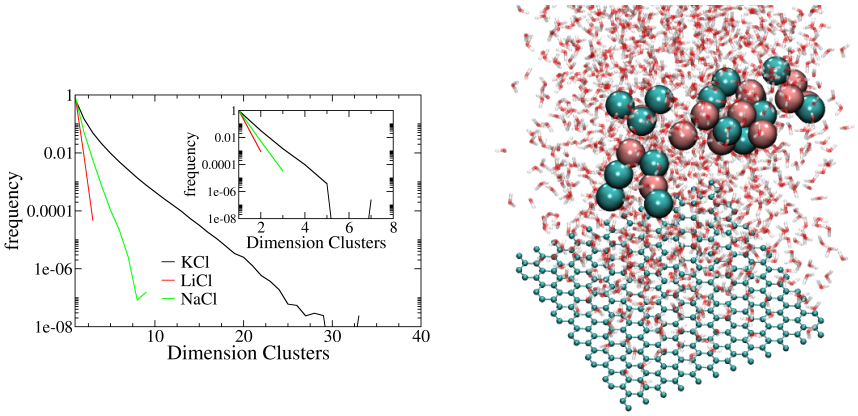

Figure 8: On the left: Histogram of the relative frequency of the cluster of different sizes for the concentration of 4.4 M. We report the histogram of the relative frequency of the cluster of different sizes for all the concentrations and systems considered in Figure S.18 of the SI. In the inset, the same quantity is reported for the 0.5 M case. On the right: an example of a cluster composed of 26 ions for the KCl system at 4.4 M.

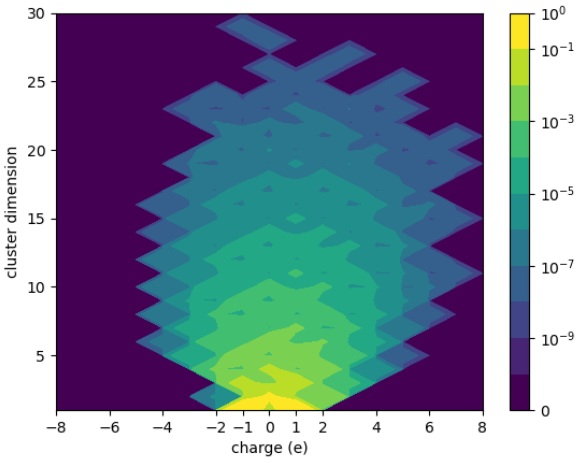

Figure 9: 2-dimensional histogram (charge VS dimension of the clusters) for the KCl(aq) system at the largest concentration considered (4.4 M).

Ion Mobilities As well as a high capacity to store charge, an optimal charge storage device must also be a good electrical conductor. In this regard, it is informative to consider how non-idealities in solution and ion association affect ion conductivities. Here, we determined the conductivity of bulk NaCl(aq) solutions from the ion diffusion coefficients calculated by Finney and Salvalaglio[64, 65]. For this purpose, we use the Nernst-Einstein equation:

$$\sigma_{NE} = \frac{e^2}{V k_{\mathrm{B}} T}(N_+ z_+^2 D_+ + N_- z_-^2 D_-) \tag{10}$$

where e, V, k_{B} and T are the elementary charge, simulation cell volume, Boltzmann's constant and temperature, respectively. N and D indicate the total number of ions and the diffusion coefficients for ions with charge indicated by the subscript, respectively. Furthermore, given the highly dynamic nature of the clusters observed in solution, we assume that the valency of ionic species, z, is equal to one.

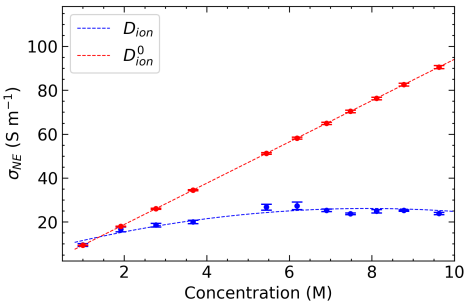

Figure 10: Solution conductivities, σ_{NE}, of bulk NaCl(aq) solutions calculated for a range of concentrations. To this aim, the Nernst-Einstein equation was adopted where ion diffusion coefficients were determined from simulations at finite concentration, D_{ion} (blue), or from a single simulation at the dilute limit, D^0_{ion} (red). Dashed lines are a guide for the eye, while error bars indicate uncertainties in the conductivities associated with the calculated D value from Refs. [64] and [65].

Suppose we assume that solutions are *ideal*. In that case, we can make use of the mean diffusion coefficient for ions evaluated in the dilute limit (D^0_{ion}) to predict the solution conductivity. For the estimate of D^0_{ion}, Finney and Salvalaglio [65] performed extended simulations of a single cation and anion embedded in a simulation cell containing 4,000 water molecules; here, $D^0_+ = 1.223 \pm 0.005 \times 10^{-5}$ cm^2 s^{-1} and $D^0_- = 1.282 \pm 0.008 \times 10^{-5}$ cm^2 s^{-1}. In addition, the diffusion coefficients were corrected to account for simulation finite size effects [66]. Unsurprisingly, a linear correlation in σ_{NE} as a function of concentration is found when a constant D^0_{ion} is used for the diffusion of ions, independent of concentration.

To determine how clustering affects the mobility of the ions and, therefore, the solution conductivity, we analysed simulations from our previous work[64] where cubic cells containing $74 - 370$ ions in $1280 - 4000$ water molecules were simulated, providing bulk solution simulations with concentrations in the range 1–10 M. As indicated in Ref. [64], ion association occurred in all simulations. This was significant at the higher end of the concentration range, leading to the formation of large liquid-like ionic networks similar to the KCl clusters described above. Figure 10 also provides the solution conductivities for NaCl(aq) computed using the Nernst-Einstein equation where the mean concentration-dependent diffusion coefficients for ions (D_{ion}) were evaluated using these simulation trajectories. Note that the diffusion of ions used in obtaining the results shown in Figure 10 was calculated for bulk solutions. There may also be surface effects on the diffusion of ions in the double layer and in bulk solution close to the electrode; nonetheless, this analysis highlights how ion clustering may affect the electrical performance of simple electrolytes at the high end of bulk concentration.

When accounting for the non-idealities in the solution and the formation of clusters explicitly in the diffusion of ions, we find that the solution conductivity reaches an upper limit between 4 and 5 M. At the lowest concentrations (1–2 M), the conductivities determined using D^0_{ion} and D_{ion} are consistent, and the simulation predictions match well with experimental measurements [67]. A crossover in the conductivity behaviour from the "pseudo-ideal" to non-ideal regime occurs between 2 and 3 M. Therefore, over a wide concentration range up to the salt solubility, non-idealities will likely affect the performance of electrical devices; depending upon the chosen application, electrolytes should be selected to minimize these effects.

4 Conclusions

In this work, we presented an extended set of simulations describing the interface between three different electrolyte solutions - (KCl(aq), LiCl(aq), and NaCl(aq)) - in contact with the surface of a negatively charged graphene electrode. To investigate these systems, we combined QM/MD and CμMD methodologies into a new simulation framework. QM/MD models of the graphene electrode in contact with an electrolyte enabled the explicit coupling of the electrode polarizability with the instantaneous configuration of the electrolyte. The latter was maintained in equilibrium with a liquid phase at constant bulk concentration thanks to the CμMD model, which mimics open-boundary conditions.

We performed a thorough analysis of the interaction of the ions with the electrode by showing the different behaviour of the three cations in the double layer, focusing on K^+, which, according to our results, can directly adsorb at the electrode surface at shorter distances compared to Li^+ and Na^+, modifying the screening effect of the solution.

Calculations of the integral capacitance indicated no concentration dependence or specific ion effects, with a total capacitance of around 4.2 µF cm^{-2} across all systems. However, the lack of variation in capacitance hides the rich electrolyte solution behaviour, particularly for the ions close to the electrode. We showed, for example, that large KCl clusters emerge in solution, which might be important when considering properties associated with ion mobility and charge transfer.

Our results indicate that accurate models of the interface - able to account for the position-dependent non-ideality of electrolyte solutions - better capture the configurational and dynamical details underpinning the electrochemical behaviour of interfaces at the atomistic level, and that is often overshadowed by the calculation of aggregated quantities such as the integral capacitance. We plan to extend our calculations to include a range of positively and negatively charged electrodes and further investigate ion dynamics in solution.

5 Supplementary Material

We are reporting here the numerical values of the potential drop in the charged and neutral electrode (see Tables S.1-S.2), a sketch of the QMMD part of the model (see Figure S.1) the radial distribution function Cations/Anions for all the systems considered (see Figure S.2), the results presented in the paper completed with errors bars for all the cases considered (the molar concentrations of cations and anions, Figure S.3-S.8; screening factors Figure S.12-S.17), the complete report for the relative frequency of the cluster size (see Figure S.18), the recalculation of the screening factor using all the charges in the electrolyte solution (see Figure S.19-S.21). We are also including and archive with the raw data containing the charge density in the box for all the systems considered.

6 Acknowledgements

We acknowledge the support provided by the IT Services use of the Computational Shared Facility (CSF) and at the University of Manchester. NDP, JDE and PC thank the European Union's Horizon 2020 research and innovation programme project VIMMP under Grant Agreement No. 760907. ARF and MS acknowledge funding from an EPSRC Programme Grant (Grant EP/R018820/1), which funds the Crystallisation in the Real World consortium.

References

[1] David Cohen-Tanugi and Jeffrey C Grossman. Water desalination across nanoporous graphene. *Nano letters*, 12(7):3602–3608, 2012.

[2] Mohammad Heiranian, Yechan Noh, and Narayana R Aluru. Dynamic and weak electric double layers in ultrathin nanopores. *The Journal of Chemical Physics*, 154(13):134703, 2021.

[3] Sumedh P Surwade, Sergei N Smirnov, Ivan V Vlassiouk, Raymond R Unocic, Gabriel M Veith, Sheng Dai, and Shannon M Mahurin. Water desalination using nanoporous single-layer graphene. *Nature nanotechnology*, 10(5):459–464, 2015.

[4] Patrice Simon and Yury Gogotsi. Materials for electrochemical capacitors. In *Nanoscience and technology: a collection of reviews from Nature journals*, pages 320–329. World Scientific, 2008.

[5] Yifan Wang, Lin Zhang, Haoqing Hou, Wenhui Xu, Gaigai Duan, Shuijian He, Kunming Liu, and Shaohua Jiang. Recent progress in carbon-based materials for supercapacitor electrodes: a review. *Journal of Materials Science*, 56(1):173–200, 2021.

[6] J. Elliott, A. A. Papaderakis, R. Dryfe, and P. Carbone. The electrochemical double layer at the graphene/aqueous electrolyte interface: what we can learn from simulations, experiments, and theory. *Journal of Materials Chemistry C*, 2022.

[7] Yan Wang, Zhiqiang Shi, Yi Huang, Yanfeng Ma, Chengyang Wang, Mingming Chen, and Yongsheng Chen. Supercapacitor devices based on graphene materials. *Journal of Physical Chemistry C*, 113(30):13103–13107, 2009.

[8] Chenguang Liu, Zhenning Yu, David Neff, Aruna Zhamu, and Bor Z Jang. Graphene-based supercapacitor with an ultrahigh energy density. *Nano letters*, 10(12):4863–4868, 2010.

[9] Aiping Yu, Isaac Roes, Aaron Davies, and Zhongwei Chen. Ultrathin, transparent, and flexible graphene films for supercapacitor application. *Applied physics letters*, 96(25):253105, 2010.

[10] Li Li Zhang, Rui Zhou, and XS Zhao. Graphene-based materials as supercapacitor electrodes. *Journal of Materials Chemistry*, 20(29):5983–5992, 2010.

[11] Y. Zhu, S. Murali, M. D. Stoller, K. J. Ganesh, W. Cai, P. J. Ferreira, A. Pirkle, R. M. Wallace, K. A. Cychosz, M. Thommes, D. Su, E. A. Stach, and R. S. Ruoff. Carbon-based supercapacitors produced by activation of graphene. *science*, 332(6037):1537–1541, 2011.

[12] Kay Hyeok An, Won Seok Kim, Young Soo Park, Young Chul Choi, Seung Mi Lee, Dong Chul Chung, Dong Jae Bae, Seong Chu Lim, and Young Hee Lee. Supercapacitors using single-walled carbon nanotube electrodes. *Advanced Materials*, 13(7):497–500, 2001.

[13] Zhoufei Yang, Jiarui Tian, Zefang Yin, Chaojie Cui, Weizhong Qian, and Fei Wei. Carbon nanotube-and graphene-based nanomaterials and applications in high-voltage supercapacitor: A review. *Carbon*, 141:467–480, 2019.

[14] C. Merlet, B. Rotenberg, P. A. Madden, and M. Salanne. Computer simulations of ionic liquids at electrochemical interfaces. *Physical Chemistry Chemical Physics*, 15(38):15781–15792, 2013.

[15] P. Iamprasertkun, W. Hirunpinyopas, A. Keerthi, B. Wang, B. Radha, M. A. Bissett, and R. A. W. Dryfe. Capacitance of basal plane and edge-oriented highly ordered pyrolytic graphite: specific ion effects. *The Journal of Physical Chemistry Letters*, 10(3):617–623, 2019.

[16] H. Yang, J. Yang, Z. Bo, X. Chen, X. Shuai, J. Kong, J. Yan, and K. Cen. Kinetic-dominated charging mechanism within representative aqueous electrolyte-based electric double-layer capacitors. *The Journal of Physical Chemistry Letters*, 8(15):3703–3710, 2017.

[17] QT Qu, B Wang, LC Yang, Y Shi, S Tian, and YP Wu. Study on electrochemical performance of activated carbon in aqueous li2so4, na2so4 and k2so4 electrolytes. *Electrochemistry Communications*, 10(10):1652–1655, 2008.

[18] J. D. Elliott, A. Troisi, and P. Carbone. A QM/MD coupling method to model the ion-induced polarization of graphene. *J. Chem. Theory Comput.*, 16(8):5253–5263, 2020.

[19] Xinran Wang, Scott M Tabakman, and Hongjie Dai. Atomic layer deposition of metal oxides on pristine and functionalized graphene. *Journal of the American Chemical Society*, 130(26):8152–8153, 2008.

[20] MJJPTA Gouy. Sur la constitution de la charge électrique à la surface d'un électrolyte. *J. Phys. Theor. Appl.*, 9(1):457–468, 1910.

[21] D. L. Chapman. LI. A contribution to the theory of electrocapillarity. *The London, Edinburgh, and Dublin philosophical magazine and journal of science*, 25(148):475–481, 1913.

[22] Otto Stern. Zur theorie der elektrolytischen doppelschicht. *Zeitschrift für Elektrochemie und angewandte physikalische Chemie*, 30(21-22):508–516, 1924.

[23] Marko Popović and Antonio Šiber. Lattice-gas poisson-boltzmann approach for sterically asymmetric electrolytes. *Physical Review E*, 88(2): 022302, 2013.

[24] Itamar Borukhov, David Andelman, and Henri Orland. Steric effects in electrolytes: A modified poisson-boltzmann equation. *Physical review letters*, 79(3):435, 1997.

[25] M. V. Fedorov and A. A. Kornyshev. Ionic liquid near a charged wall: Structure and capacitance of electrical double layer. *The Journal of Physical Chemistry B*, 112(38):11868–11872, aug 2008. doi: 10.1021/jp803440q.

[26] J. J. Howard, J. S. Perkyns, and B. M. Pettitt. The behavior of ions near a charged wall-dependence on ion size, concentration, and surface charge. *The journal of physical chemistry B*, 114(18):6074–6083, 2010.

[27] Rahul Prasanna Misra and Daniel Blankschtein. Ion adsorption at solid/water interfaces: Establishing the coupled nature of ion–solid and water–solid interactions. *The Journal of Physical Chemistry C*, 125(4): 2666–2679, 2021.

[28] C. Perego, M. Salvalaglio, and M. Parrinello. Molecular dynamics simulations of solutions at constant chemical potential. *The Journal of Chemical Physics*, 142(14):144113, apr 2015. doi: 10.1063/1.4917200.

[29] Aaron R Finney, Ian J McPherson, Patrick R Unwin, and Matteo Salvalaglio. Electrochemistry, ion adsorption and dynamics in the double layer: a study of nacl (aq) on graphite. *Chemical science*, 12(33):11166–11180, 2021.

[30] K. Doblhoff-Dier and M. T. M. Koper. Modeling the Gouy–Chapman diffuse capacitance with attractive ion–surface interaction. *The Journal of Physical Chemistry C*, 125(30):16664–16673, 2021.

[31] Arthur France-Lanord and Jeffrey C Grossman. Correlations from ion pairing and the nernst-einstein equation. *Physical review letters*, 122(13): 136001, 2019.

[32] Rahul Prasanna Misra and Daniel Blankschtein. Uncovering a Universal Molecular Mechanism of Salt Ion Adsorption at Solid/Water Interfaces. *Langmuir*, 37(2):722–733, January 2021.

[33] C. D. Williams, J. Dix, A. Troisi, and P. Carbone. Effective Polarization in Pairwise Potentials at the Graphene–Electrolyte Interface. *J. Phys. Chem. Lett.*, 8(3):703, February 2017.

[34] J Ilja Siepmann and Michiel Sprik. Influence of surface topology and electrostatic potential on water/electrode systems. *The Journal of chemical physics*, 102(1):511, 1995.

[35] Alessandro Coretti, Camille Bacon, Roxanne Berthin, Alessandra Serva, Laura Scalfi, Iurii Chubak, Kateryna Goloviznina, Matthieu Haefele, Abel Marin-Laflèche, Benjamin Rotenberg, et al. Metalwalls: Simulating electrochemical interfaces between polarizable electrolytes and metallic electrodes. *The Journal of Chemical Physics*, 157(18):184801, 2022.

[36] Céline Merlet, Clarisse Péan, Benjamin Rotenberg, Paul Anthony Madden, Barbara Daffos, P-L Taberna, Patrice Simon, and Mathieu Salanne. Highly confined ions store charge more efficiently in supercapacitors. *Nature communications*, 4(1):1–6, 2013.

[37] Céline Merlet, Benjamin Rotenberg, Paul A Madden, Pierre-Louis Taberna, Patrice Simon, Yury Gogotsi, and Mathieu Salanne. On the molecular origin of supercapacitance in nanoporous carbon electrodes. *Nature materials*, 11(4):306–310, 2012.

[38] Laura Scalfi, Thomas Dufils, Kyle G Reeves, Benjamin Rotenberg, and Mathieu Salanne. A semiclassical thomas–fermi model to tune the metallicity of electrodes in molecular simulations. *The Journal of Chemical Physics*, 153(17):174704, 2020.

[39] Alessandro Landi, Maryam Reisjalali, Joshua D Elliott, Micaela Matta, Paola Carbone, and Alessandro Troisi. Simulation of polymeric mixed ionic and electronic conductors with a combined classical and quantum mechanical model. *Journal of Materials Chemistry C*, 2023.

[40] Nicodemo Di Pasquale, Joshua D Elliott, Panagiotis Hadjidoukas, and Paola Carbone. Dynamically polarizable force fields for surface simulations via multi-output classification neural networks. *Journal of Chemical Theory and Computation*, 17(7):4477–4485, 2021.

[41] M. J. Abraham, T. Murtola, R. Schulz, S. Páll, J. C. Smith, B. Hess, and E. Lindahl. GROMACS: High performance molecular simulations through multi-level parallelism from laptops to supercomputers. *SoftwareX*, 1:19–25, 2015.

[42] G. A. Tribello, M. Bonomi, D. Branduardi, C. Camilloni, and G. Bussi. Plumed 2: New feathers for an old bird. *Computer physics communications*, 185(2):604–613, 2014.

[43] B. Hourahine, B. Aradi, V. Blum, F. Bonafé, A. Buccheri, C. Camacho, C. Cevallos, M. Y. Deshaye, T. Dumitrică, A. Dominguez, S. Ehlert, M. Elstner, T. van der Heide, J. Hermann, S. Irle, J. J. Kranz, C. Köhler, T. Kowalczyk, T. Kubař, I. S. Lee, V. Lutsker, R. J. Maurer, S. K. Min, I. Mitchell, C. Negre, T. A. Niehaus, A. M. N. Niklasson, A. J. Page, A. Pecchia, G. Penazzi, M. P. Persson, J. Řezáč, C. G. Sánchez, M. Sternberg, M. Stöhr, F. Stuckenberg, A. Tkatchenko, V. W.-z. Yu, and T. Frauenheim. DFTB+, a software package for efficient approximate density functional theory based atomistic simulations. *The Journal of Chemical Physics*, 152 (12):124101, 2020. doi: 10.1063/1.5143190.

[44] J. D. Elliott, M. Chiricotto, A. Troisi, and P. Carbone. Do specific ion effects influence the physical chemistry of aqueous graphene-based supercapacitors? perspectives from multiscale qmmd simulations. *arXiv*, 2022. doi: 10.48550/ARXIV.2203.02469.

[45] Marcus Elstner, Dirk Porezag, G Jungnickel, J Elsner, M Haugk, Th Frauenheim, Sandor Suhai, and Gotthard Seifert. Self-consistent-charge density-functional tight-binding method for simulations of complex materials properties. *Physical Review B*, 58(11):7260, 1998.

[46] William M Haynes, David R Lide, and Thomas J Bruno. *CRC handbook of chemistry and physics*. CRC press, 2016.

[47] I. M. Zeron, J. L. F. Abascal, and C. Vega. A force field of Li^+, Na^+, K+, Mg^{2+}, Ca^{2+}, Cl^-, and SO_4^{2-} in aqueous solution based on the TIP4P/2005 water model and scaled charges for the ions. *The Journal of chemical physics*, 151(13):134504, 2019.

[48] Tuan A Ho and Alberto Striolo. Capacitance enhancement via electrode patterning. *The Journal of Chemical Physics*, 139(20):204708, 2013.

[49] Kui Xu, Hui Shao, Zifeng Lin, Céline Merlet, Guang Feng, Jixin Zhu, and Patrice Simon. Computational insights into charge storage mechanisms of supercapacitors. *Energy & environmental materials*, 3(3):235–246, 2020.

[50] Robert S Mulliken. Electronic population analysis on lcao–mo molecular wave functions. i. *The Journal of Chemical Physics*, 23(10):1833–1840, 1955.

[51] H. J. C. Berendsen, D. van der Spoel, and R. van Drunen. Gromacs: a message-passing parallel molecular dynamics implementation. *Computer physics communications*, 91(1-3):43–56, 1995.

[52] D. van der Spoel, E. Lindhal, B. Hess, G. Groenhof, A. E. Mark, and H. J. C. Berendsen. Gromacs: Fast, flexible and free. *J. Comput. Chem.*, 26(16):1701–1718, 2005.

[53] H. J. C. Berendsen, J. R. Grigera, and T. P. Straatsma. The missing term in effective pair potentials. *Journal of Physical Chemistry*, 91(24):6269–6271, 1987.

[54] S. Miyamoto and P. A. Kollman. SETTLE: An analytical version of the SHAKE and RATTLE algorithm for rigid water molecules. *J. Comput. Chem*, 13:952–962, 1992.

[55] Yi Huang, Jiajie Liang, and Yongsheng Chen. An overview of the applications of graphene-based materials in supercapacitors. *small*, 8(12): 1805–1834, 2012.

[56] I. S. Joung and T. E. III Cheatham. Determination of alkali and halide monovalent ion parameters for use in explicitly solvated biomolecular simulations. *The journal of physical chemistry B*, 112(30):9020–9041, 2008.

[57] Aric Hagberg, Pieter Swart, and Daniel S Chult. Exploring network structure, dynamics, and function using networkx. Technical report, Los Alamos National Lab.(LANL), Los Alamos, NM (United States), 2008.

[58] M. F. Döpke, O. A. Moultos, and R. Hartkamp. On the transferability of ion parameters to the tip4p/2005 water model using molecular dynamics simulations. *The Journal of chemical physics*, 152(2):024501, 2020.

[59] J. Dočkal, M. Lísal, and F. Moučka. Molecular dynamics of the interfacial solution structure of alkali-halide electrolytes at graphene electrodes. *Journal of Molecular Liquids*, 353:118776, 2022.

[60] Jan Dočkal, Filip Moučka, and Martin Lísal. Molecular Dynamics of Graphene–Electrolyte Interface: Interfacial Solution Structure and Molecular Diffusion. *J Phys. Chem. C*, 123(43):26379, October 2019.

[61] Alexei A Kornyshev. Double-layer in ionic liquids: paradigm change? *The Journal of Physical Chemistry B*, 111(20):5545–5557, 2007.

[62] Ian Snook and William van Megen. Finite ion size effects in the electrical double layer—a monte carlo study. *The Journal of Chemical Physics*, 75 (8):4104–4106, 1981.

[63] Hyerim Hwang, Yong Chan Cho, Sooheyong Lee, Yun-Hee Lee, Seongheun Kim, Yongjae Kim, Wonhyuk Jo, Patrick Duchstein, Dirk Zahn, and Geun Woo Lee. Hydration breaking and chemical ordering in a levitated NaCl solution droplet beyond the metastable zone width limit: evidence for the early stage of two-step nucleation. *Chemical Science*, 12(1):179–187, 2021. doi: 10.1039/d0sc04817h. URL `https://doi.org/10.1039%2Fd0sc04817h`.

[64] Aaron R Finney and Matteo Salvalaglio. Multiple pathways in nacl homogeneous crystal nucleation. *Faraday Discussions*, 2022.

[65] A. R. Finney and M. Salvalaglio. Bridging the gap between mesoscopic and molecular models of solid/liquid interfaces out-of-equilibrium. *arXiv preprint arXiv:2109.00568*, 2021.

[66] I. Yeh and G. Hummer. System-Size Dependence of Diffusion Coefficients and Viscosities from Molecular Dynamics Simulations with Periodic Boundary Conditions. *The Journal of Physical Chemistry B*, 108(40):15873–15879, October 2004.

[67] C. S. Widodo, H. Sela, and D. R. Santosa. The effect of nacl concentration on the ionic nacl solutions electrical impedance value using electrochemical impedance spectroscopy methods. In *AIP Conference Proceedings*, volume 2021, page 050003. AIP Publishing LLC, 2018.